OPEN ACCESS

The role of hydrogen in room-temperature ferromagnetism at graphite surfaces

New Journal of Physics
The open-access journal for physics

The role of hydrogen in room-temperature ferromagnetism at graphite surfaces

H Ohldag[1,4], P Esquinazi[2], E Arenholz[3], D Spemann[2], M Rothermel[2], A Setzer[2] and T Butz[2]

[1] Stanford Synchrotron Radiation Lightsource, Stanford University, Menlo Park, CA 94025, USA
[2] Institut für Experimentelle Physik II, Universität Leipzig, Linnéstraße 5, 04103 Leipzig, Germany
[3] Advanced Light Source, Lawrence Berkeley National Laboratory, Berkeley, CA 94720, USA
E-mail: hohldag@stanford.edu

New Journal of Physics **12** (2010) 123012 (10pp)
Received 17 May 2010
Published 8 December 2010
Online at http://www.njp.org/
doi:10.1088/1367-2630/12/12/123012

Abstract. We present an x-ray dichroism study of graphite surfaces that addresses the origin and magnitude of ferromagnetism in metal-free carbon. We find that, in addition to carbon π-states, hydrogen-mediated electronic states also exhibit a net spin polarization with significant magnetic remanence at room temperature. The observed magnetism is restricted to the top $\approx$10 nm of the irradiated sample where the average magnetization reaches $\simeq$15 emu g^{-1} at room temperature. We prove that the ferromagnetism found in metal-free untreated graphite is intrinsic and has a similar origin to that found in proton-bombarded graphite. Our findings also show that the magnetic properties of graphite surfaces, thin films or two-dimensional graphene samples can be reliably studied using soft x-ray dichroism. Fundamental new insights into the magnetic properties of carbon-based systems can thus be obtained.

The possibility of magnetic order in metal-free carbon is fascinating from a fundamental as well as from a technological point of view. In recent years, there have been numerous reports of ferromagnetism in untreated graphite [1], as well as graphite treated by ion bombardment [2]–[4] and carbon nanoparticles [5]–[7]; it could be shown that the observed magnetism in proton-irradiated carbon is not caused by magnetic impurities but is related to the

[4] Author to whom any correspondence should be addressed.

π-states of carbon [8]. However, the question of how it is possible to establish ferromagnetic order in carbon without any metallic magnetic or non-magnetic elements remains unanswered. Several theoretical studies in the past have suggested that absorption of hydrogen at the edges of [9] or on [10] graphene sheets, as well as hydrogen chemisorption in graphite [11], may lead to the formation of a spin-polarized band at the Fermi level and robust ferromagnetic order. However, there is so far no convincing experimental evidence supporting the influence of hydrogen. While it is obvious that defects or adatoms play a vital role, the origin of the magnetic moment observed in graphite [1] is not yet understood.

Another intriguing question arises from the observation that the apparent magnetization detected in magnetic graphite is typically many orders of magnitude smaller than that found for 'classical' magnets such as three-dimensional (3D) transition metals. Apart from the fact that this makes it challenging to obtain a reliable and detailed understanding of the relevant processes that cause ferromagnetic order in graphite [12], it also leads to the question of how such a system exhibiting small magnetization and presumably negligible magnetic exchange coupling can be a ferromagnet at room temperature. The explanation for such extremely small magnetization resides in the uncertainty of the total ferromagnetic mass in the measured samples and in the role of non-metallic defects. Recent studies on proton- [3] and carbon-irradiated [4] graphite managed to provide maximum limits for the induced ferromagnetic mass, allowing one to estimate magnetization values exceeding $5\,\mathrm{emu\,g^{-1}}$. Although important evidence has been obtained that supports the role of vacancies in the graphite ferromagnetism [13], the very origin and extent of surface magnetism [14] remains open. For this reason, we will investigate the electronic structure of such samples and correlate our findings with the macroscopic magnetic properties.

In this paper, we present x-ray absorption (XA) and x-ray magnetic circular dichroism (XMCD) spectra in combination with superconducting quantum interference device (SQUID) measurements on proton-irradiated as well as untreated highly oriented pyrolytic graphite (HOPG) samples. Soft XA dichroism spectroscopy is an element-specific technique that is sensitive to the magnetic moment of each elemental or chemical species in a complex heterogeneous sample. The x-ray energy is chosen such that core-level electrons are excited into empty valence states. Using circularly polarized x-rays, the intensity of the absorption process in a magnetic element depends on the relative orientation between the helicity of the x-rays and the magnetic moment of the atom (XMCD) [15]. To obtain an XMCD spectrum two XA spectra with either opposite magnetization or x-ray polarization [16] are recorded and compared. It is important to note that XMCD can provide independent information about the magnetic order of different elements or even different chemical states of one element in a sample. Furthermore, it is possible to change the depth sensitivity of the approach by using different detection methods for the absorption yield. We will employ exactly these capabilities of XMCD to show that hydrogen atoms at the surface of graphite play a key role in the ferromagnetism of graphite and that the size of the magnetic moment of graphite at the surface can reach the same order of magnitude as classical ferromagnetic materials.

The XA experiments were performed using the eight-pole magnet [17] at the elliptically polarized undulator beamline 4.0.2 at the Advanced Light Source in Berkeley [18] at room temperature. The x-ray source provides soft x-rays in the energy range between 250 and 2000 eV with a typical spectral resolution of $E/\Delta E \approx 5000$. The photon energy of the x-ray beam has been calibrated using well-known absorption resonances. The source provides x-rays with variable orientation and phase of the electric field vector (circular/linear) and a

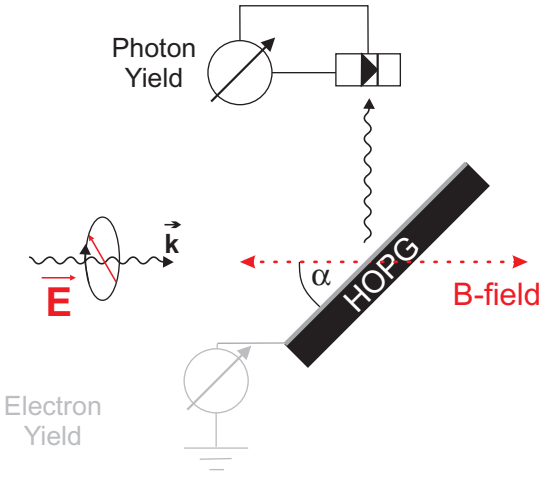

Figure 1. Experimental geometry. Circularly polarized x-rays are incident on the sample under an angle α collinear with the direction of the applied magnetic field. A photodiode at 90° to the incoming x-rays can be used to measure the reflected x-ray intensity at $\alpha = 45°$. The absorption yield is measured by monitoring the sample drain current.

Table 1. Metallic impurities in the two HOPG samples investigated here measured in ppm (1 ppm = 1 μg element per gram carbon) using PIXE.

Sample	Ti	V	Cr	Fe	Co	Ni	Cu	Zn
Irradiated	3.56	7.1	< 0.03	0.25	< 0.02	0.11	0.4	0.3
Virgin	2.69	8.52	0.11	0.61	$\simeq 0$	0.13	0.06	$\lesssim 0.06$

high degree of polarization. The electromagnet provides a magnetic field that was applied parallel to the direction of the incoming x-rays, while the sample was oriented at an angle α, as shown in figure 1. At $\alpha = 30°$, only the electron yield (EY) emitted from the sample was recorded, while we also recorded the reflected x-ray intensity (reflection yield, RY) at $\alpha = 45°$ using a photodiode. The EY approach provides surface-specific information from the first 5–10 nm of the sample [16], while the reflected photons provide more bulk-sensitive information (0.1–1 μm) [19]. XMCD spectra were obtained by switching the direction of the applied field for every data point. The EY and RY data were recorded in an applied field or in remanence after the field was removed.

The two samples discussed in this paper were obtained from an HOPG (0.4° rocking curve width) bulk sample. The negligible amount of magnetic impurities such as Fe, Co and Ni in our samples was confirmed by using particle-induced x-ray emission (PIXE). The results are summarized in table 1. The total amount of metallic impurities in the bulk of both samples is of the order of 10 ppm (10 μg per gram carbon); however, the concentration for each of the magnetic elements is well below 1 ppm. To exclude that the metallic impurities detected by PIXE are not exclusively located within the surface; we also acquired XA spectra between 200 and 1500 eV (not shown), covering the absorption resonances of the 3d metals Cr, V, Mn, Fe, Co, Ni and Cu, as well as Gd. The XA spectra did not show any indication of metallic

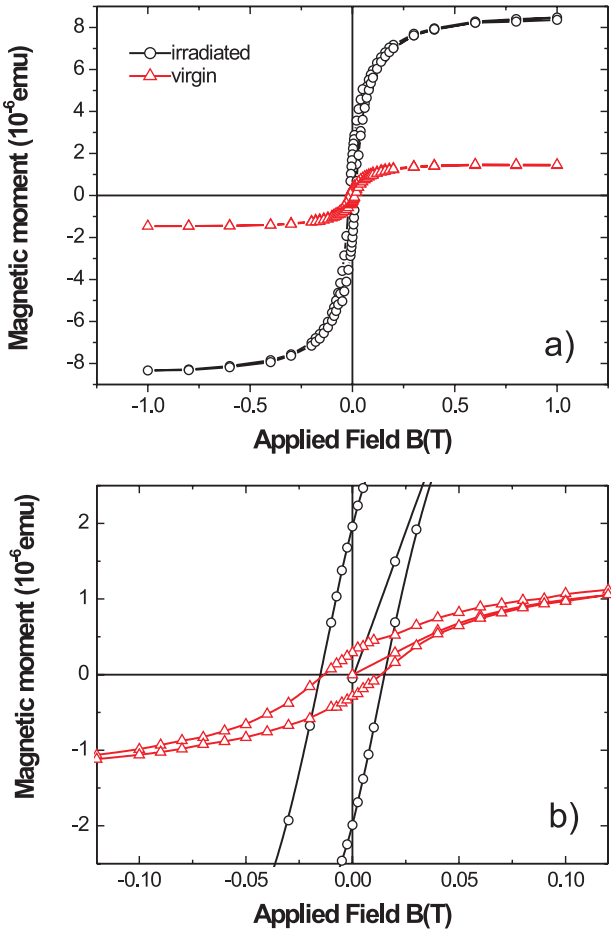

Figure 2. (a) Hysteresis loops (magnetic moment m versus applied field B) measured with SQUID at 300 K for the irradiated (black) and virgin (red) HOPG samples of identical areas and after subtraction of a linear diamagnetic background (field applied $\perp$ the c-axis) (b) The low-field region of the hysteresis loop is shown to demonstrate magnetic remanence and coercivity of the two samples.

impurities in the surface layers. While one sample, in the following referred to as the virgin sample, was not treated any further, the other sample was irradiated with a relatively weak fluence of 0.1 nC μm^{-2} protons of 2 MeV energy (180 nA ion current). Hysteresis loops of the measured moments from the two samples are shown in figure 2. Both hysteresis loops show features that are indicative of ferromagnetic order, such as magnetic saturation at low fields ($\lesssim$0.5 T), magnetic remanence at zero field and the existence of a non-vanishing coercive field that is needed to reverse the magnetization into the opposite direction. To illustrate all of these three points we show the overview loops in figure 2(a), as well as a magnified view of the low-field region of the hysteresis loop in figure 2(b). We would like to point out that the XA spectra did show the presence of oxygen at the surface of HOPG, due to the fact that the samples were exposed to air during transport and mounting. From the intensity of the oxygen peak in the XA spectrum, we can conclude that the contamination is well below a monolayer.

Carbon K-edge soft XA spectra of the virgin and irradiated HOPG samples obtained using EY detection at an angle of incidence $\alpha = 30^\circ$ using circular polarization are shown in figure 3(a). The XA spectrum of the virgin sample shows a narrow resonance at 285.3 eV and a broader resonance around 293 eV, which represent the well-known excitation of 1s core-level electrons into empty $\pi^\star$ and $\sigma^\star$ bands [20], respectively. The additional feature at the onset of the $\sigma^\star$ resonance results from an excitonic transition [21]. The $\pi^\star$ and $\sigma^\star$ features are much broader in the spectra of the irradiated sample, and in particular the intensity of the $\pi^\star$ resonance is greatly reduced, a sign that the irradiated sample is more disordered. This observation is consistent with previous microscopy [8] and Raman studies [22], in which we directly compared irradiated and non-irradiated areas on a carbon sample.

The lower panel of figure 3(a) shows the XMCD spectrum obtained in an applied magnetic field of ± 0.5 T using circularly polarized x-rays. To plot the XMCD difference, which is on average less than 1% of the XA intensity, on the same scale as the XA spectrum, we multiplied it by a factor of 100. The excellent signal-to-noise ratio is achieved by averaging the XMCD difference over several scans. Surprisingly, the onset of the absorption yield, as well as the XMCD intensity, lies well below the $\pi^\star$-resonance between 270 and 275 eV. In our spectra, the Fermi level appears at about 283 eV, which means that the XMCD and XA signals extend to about 10 eV below E_F. However, the possibility that dichroism in soft XA may appear already below the Fermi level has been previously reported by Mertins *et al* [23], who have shown that dichroic effects of non-magnetic origin can indeed be experimentally observed as low as 270 eV in the carbon 1s XA spectrum. A theoretical description of pre-edge dichroism effects is still elusive and beyond the scope of this paper. We expect, however, that the fact that such effects have now been reported repeatedly will stimulate future theoretical work on this matter.

The broad pre-edge peak of the XMCD spectrum in figure 3 exhibits an absolute maximum at about 3 eV below E_F. The energy range for which the pre-edge XMCD is observed is consistent with the energy spread of the carbon π-bands and the maximum of the XMCD at $\simeq$280 eV corresponds to the valence band maximum π valence band (VB_{max}); see for example [24]. The XMCD spectra of both samples also show a positive peak at 284 eV at the onset of the $\pi^\star$-resonance close to the Fermi level. Previous theoretical investigations predicted the occurrence of a spin-polarized band due to H chemisorption [9]–[11] at this energy, which we now observe in our XA spectrum. Since the observed spectral differences are very small, about 1% of the total XA intensity, it is crucial to corroborate that they indeed represent a magnetic circular dichroism and are not due to systematic asymmetries. For this reason, we acquired difference spectra by either switching the magnetization for each data point (constant x-ray polarization, red and green line) or by switching the x-ray polarization for each data point (constant magnetic field, black and blue spectra). The resulting four difference spectra are shown in figure 3(b). No averaging has been applied to these spectra, which explains the higher noise level compared to figure 3(a). The four spectra are quantitatively identical, except for the sign, indicating that the observed dichroism is a true XMCD effect that reverses its sign upon switching the direction of the x-ray polarization or the direction of the magnetization. There is no intrinsic or systematic and non-magnetic dichroism present in our sample or setup, e.g. due to chiral coordination around the carbon sites or asymmetric polarization properties of the x-ray source.

The XMCD spectrum of the irradiated sample shows an additional feature around 286 eV. X-ray studies of single-walled carbon nanotubes [25] and graphite surfaces [26] have shown that C–H bond formation will occur through re-hybridization of carbon sp^2 bonds to sp^3 bonds

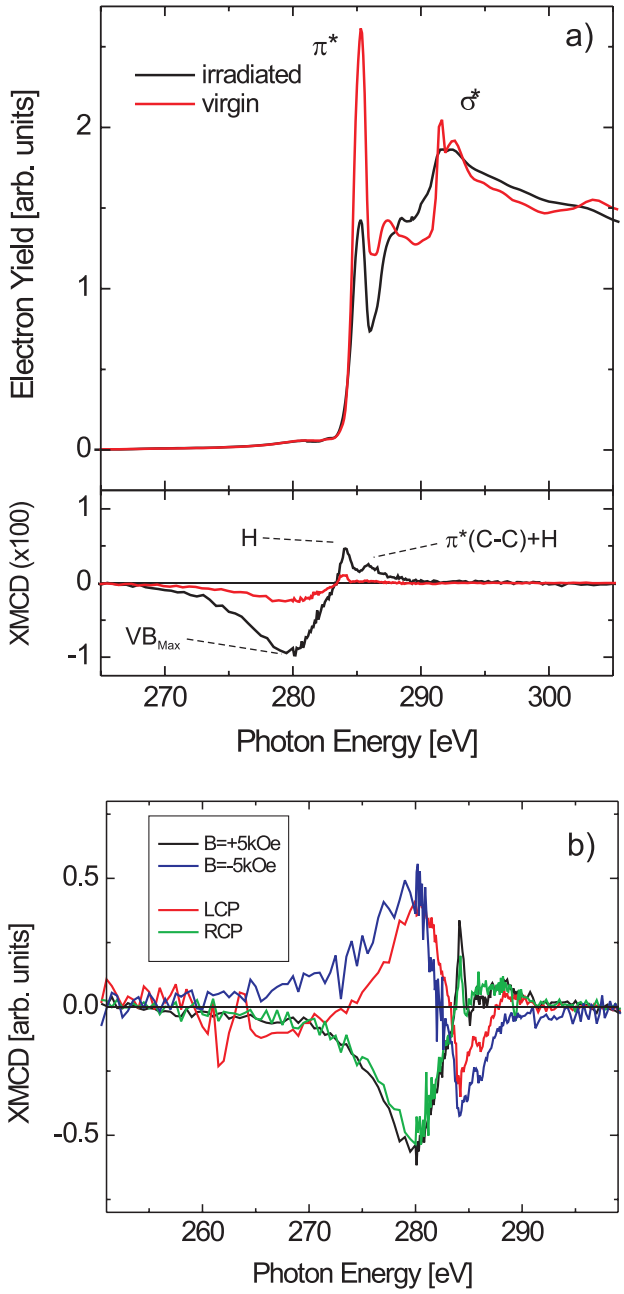

Figure 3. (a) XA spectra of the irradiated (black) and virgin (red) HOPG samples measured using EY, as well as the XMCD difference ($\times 100$) detected using an applied field of ± 0.5 T. The spectra were obtained at 30° grazing incidence using circular polarization. (b) A full set of XMCD difference spectra of the irradiated sample measured by switching either the x-ray polarization or the applied magnetic field for every data point. The black and blue spectra were obtained by switching the polarization for each data point between left and right circularly polarized (LCP and RCP), while keeping the external magnetic field constant, either +5 kOe (black) or −5 kOe (blue). The red and green difference spectra were obtained by keeping the orientation of the x-ray polarization constant but switching the external magnetic field for each data point.

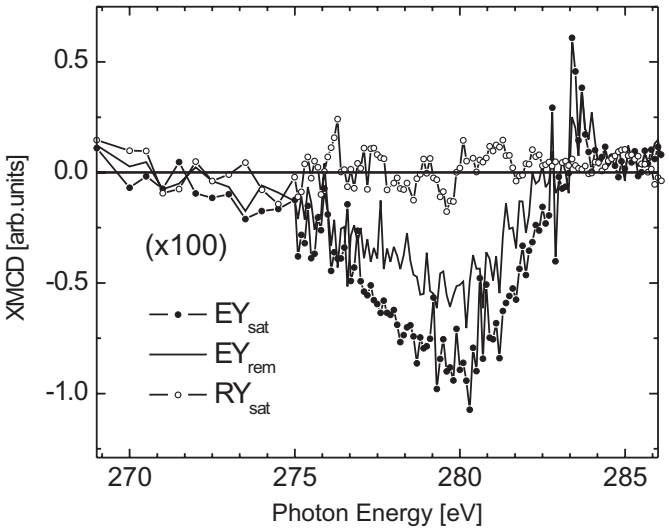

Figure 4. XMCD spectra ($\times 100$) of the irradiated HOPG samples obtained using EY in an applied field of ± 0.7 T (•) or in remanence after saturating the sample in a field of ± 0.7 T (−). Also shown is the XMCD spectrum acquired in saturation using the RY (○). Lines are added as a guide to the eye. All spectra were obtained at $\alpha = 45^{\circ}$.

by attachment of hydrogen, leading to a resonance in the XA spectrum about 1 eV above the $\pi^{\star}$-resonance. We find that both the hydrogen band and the re-hybridized sp^3 carbon π-band exhibit a magnetic moment in the irradiated sample. The sp^3 feature, however, is absent in the XMCD spectrum of the virgin sample, while the feature at 284 eV is again a factor of $\sim$4 smaller. Combined, these observations indicate that the effect of proton irradiation is the incorporation of hydrogen through re-hybridization. This may initially be advantageous for the evolution and stabilization of ferromagnetism in graphite. However, it also becomes evident that intense proton irradiation, in particular at ambient temperatures, will significantly enhance the diffusion of H and also disturb the crystallographic and hence the electronic structure of graphite, reducing the magnetic order. We note that no XMCD intensity is observed at photon energies correlated with the presence of surface oxides around 289 eV, excluding the possibility that surface oxidation plays a significant role in the ferromagnetism of graphite.

Figure 4 shows three XMCD spectra (no averaging as in figure 3(a)) obtained from the irradiated sample. The spectra were acquired at an angle of incidence $\alpha = 45^{\circ}$, so that the intensity of the RY could be detected at the same time as the EY in our setup. The RY provides bulk-sensitive information, while the EY is a surface-sensitive approach. This is, in particular, true at energies below the π-resonance around 280 eV where the absorption cross section is small and the x-rays can penetrate deeper into the material, while the escape depth of the secondary electrons contributing to the EY remains small. The XMCD signal acquired using EY shows the prominent feature at 280 eV, which clearly persists after the external field is removed, showing a clear magnetic remanence of about 60% of the saturation value. On the other hand, there is no XMCD detected in the RY spectrum in figure 4. If the magnetization persisted into the bulk without any change of magnitude it would be visible in the RY differences at 280 or 284 eV. Therefore, taking into account the different probing depths of the two approaches

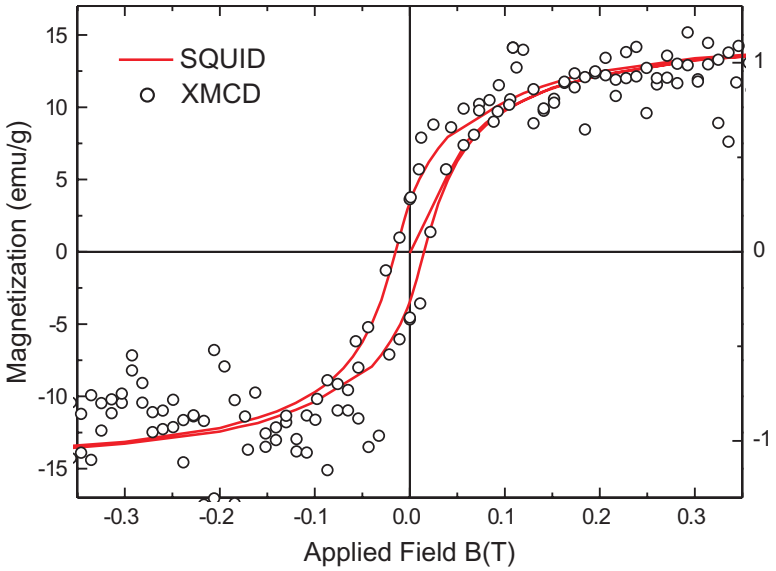

Figure 5. Hysteresis loops of the irradiated sample acquired using SQUID (−) or XMCD (○). The axis on the left side shows the magnetization of the sample in emu g^{-1}. The axis on the right for the XMCD loop is chosen such that the saturation values coincide for comparison.

between 280 and 284 eV (10 nm for EY [20] versus 0.1–1 μm for RY [19]), we can conclude that the observed ferromagnetism in the irradiated sample originates predominantly from the top 10 nm of the sample.

Note that because of the limited signal-to-noise ratio and sensitivity of the approach we do not exclude the existence of ferromagnetic order in the bulk of the sample. We estimate, however, that more than 80% of the magnetic moment of the irradiated sample that is observed via the SQUID is located within the first 10 nm of the sample.

The fact that the majority of the magnetic moment originates from the surface allows us to provide an estimate for the true magnetization values of the HOPG surface now by normalizing the magnetic moment obtained by the SQUID hysteresis loop in figure 3(a) with the correct thickness of the magnetic layer. We find that the average saturation magnetization for the irradiated sample within the top 10 nm is of the order of 15 emu g^{-1}. But the actual magnetization of the layers closest to the surface may be even higher, up to 45 emu g^{-1}, assuming that the magnetization reaches its maximum at the surface and decays exponentially into the bulk of the material, so that again ∼80% of the total magnetization is within the first 10 nm. Figure 5 shows the corrected SQUID hysteresis loop—assuming the simple case—displaying the magnetization of the sample surface. For comparison, the magnetic moment of Fe is about 220 emu g^{-1}, or 55 emu g^{-1} for Ni, which means that the magnetization at the surface of HOPG is similar to bulk magnetization of Ni metal. Note that a direct determination of the total magnetic moment (spin and orbit) of the carbon atoms using XA sum rules is not possible because the carbon K-edge XMCD only probes the orbital moment. Nevertheless, both techniques (SQUID and XMCD) measure the same macroscopic magnetic properties. For comparison, we show a hysteresis loop obtained using XMCD at a photon energy of 280 eV in figure 5, which follows the SQUID hysteresis loop nicely.

In conclusion, we report the observation of ferromagnetic order at surfaces of metal-free HOPG before and after proton irradiation. The results in virgin HOPG clearly indicate that the observed ferromagnetism in untreated, pure graphite [1] is intrinsic. We find that the observed XMCD signal originates mostly from the near-surface region ($\approx$10 nm) of the sample, where the saturation magnetization may reach up to 25% of that of Ni. The rather large magnetic moment of ferromagnetic HOPG is now consistent with the occurrence of room-temperature ferromagnetism. Furthermore, it points to the possibility that the magnetic properties of carbon can indeed play a significant role in bio-compatible nanoapplications, as well as an organic magnetic 'substrate' in chiral selective chemistry [27]. The XMCD line shape shows that chemisorbed hydrogen and C–H bond states, as well as carbon π-states, exhibit a net spin polarization. While the proton irradiation initially increases the magnetic moment by the formation of C–H bonds, it also disturbs the system for the same reason by introducing disorder and formation of sp^3-bonds, providing an explanation of the limit to which the magnetization in carbon can be increased by ion irradiation. Our results also indicate that hydrogen is not implanted—the implantation probability of 2 MeV photons is very small at the surface—but should come from dissociation of H_2 molecules by the proton irradiation, since a large hydrogen concentration is always present in the near-surface region [28].

Acknowledgments

HO thanks Joachim Stöhr and Hans-Christoph Siegmann for their support and stimulating discussions. SSRL and ALS are national user facilities supported by the Department of Energy, Office of Basic Energy Sciences. SSRL is operated by Stanford University and ALS is operated by the University of California under contract no. DE-AC02-05CH11231. The work at the University of Leipzig is supported by the DFG under DFG ES 86/16-1.

References

[1] Esquinazi P, Setzer A, Höhne R, Semmelhack C, Kopelevich Y, Spemann D, Butz T, Kohlstrunk B and Lösche M 2002 Ferromagnetism in oriented graphite samples *Phys. Rev.* B **66** 024429
[2] Esquinazi P, Spemann D, Höhne R, Setzer A, Han K-H and Butz T 2003 Induced magnetic ordering by proton irradiation in graphite *Phys. Rev. Lett.* **91** 227201
[3] Barzola-Quiquia J, Esquinazi P, Rothermel M, Spemann D, Butz T and García N 2007 Experimental evidence for two-dimensional magnetic order in proton bombarded graphite *Phys. Rev.* B **76** 161403
[4] Xia H *et al* 2008 Tunable magnetism in carbon-ion-implanted highly oriented pyrolytic graphite *Adv. Mater.* **20** 1–5
[5] Kopelevich Y, da Silva R R, Torres J H S, Penicaud A and Kyotani T 2003 Local ferromagnetism in microporous carbon with the structural regularity of zeolite Y *Phys. Rev.* B **68** 092408
[6] Caudillo R, Gao X, Escudero R, José-Yacaman M and Goodenough J B 2006 Ferromagnetic behavior of carbon nanospheres encapsulating silver nanoparticles *Phys. Rev.* B **74** 214418
[7] Parkanskya N, Alterkopa B, Boxmana R L, Leitusb G, Berkhc O, Barkayd Z, Rosenberg Y and Eliaz N 2008 Magnetic properties of carbon nano-particles produced by a pulsed arc submerged in ethanol *Carbon* **46** 215–9
[8] Ohldag H, Tylisczak T, Höhne R, Spemann D, Esquinazi P, Ungureanu M and Butz T 2007 π-Electron ferromagnetism in metal-free carbon probed by soft x-ray dichroism *Phys. Rev. Lett.* **98** 187204
[9] Kusakabe K and Maruyama M 2003 Magnetic nanographite *Phys. Rev.* B **67** 092406
[10] Duplock E J, Scheffler M and Lindan P J D 2004 Hallmark of perfect graphite *Phys. Rev. Lett.* **92** 225502

[11] Yazyev O V 2008 Magnetism in disordered graphene and irradiated graphite *Phys. Rev. Lett.* **101** 037203
[12] Esquinazi P, Barzola-Quiquia J, Spemann D, Rothermel M, Ohldag H, García N, Setzer A and Butz T 2008 Magnetic order in graphite: experimental evidence, intrinsic and extrinsic difficulties *J. Magn. Magn. Mater.* **322** 1156–61
[13] Yanga X, Xiab H, Qinc X, Lia W, Daia Y, Liua X, Zhaoa M, Xiaa Y, Yana S and Wangc B 2009 Correlation between the vacancy defects and ferromagnetism in graphite *Carbon* **47** 1399–406
[14] Dubman M *et al* 2010 Low-energy μSR and SQUID evidence of magnetism in highly oriented pyrolytic graphite *J. Magn. Magn. Mater.* **322** 1228–31
[15] Thole B T, Carra P, Sette F and der Laan G 1992 X-ray circular dichroism as a probe of orbital magnetism *Phys. Rev. Lett.* **68** 1943
[16] Stöhr J and Siegmann H C 2006 *Magnetism—From Fundamentals to Nanoscale Dynamics* (*Springer Series in Solid State Sciences* vol 152) (Heidelberg: Springer)
[17] Arenholz E and Prestomon S 2005 Design and performance of an eight-pole resistive magnet for soft x-ray magnetic dichroism measurements *Rev. Sci. Instrum.* **76** 083908
[18] Young A, Arenholz E, Marks S, Schlueter R, Steier C, Padmore H, Hitchcock A and Castner D 2002 Variable linear polarization from an x-ray undulator *J. Synchrotron. Radiat.* **9** 270
[19] For example, see http://henke.lbl.gov/optical_constants/atten2.html
[20] Stöhr J 1992 *NEXAFS Spectroscopy* (*Springer Series in Surface Science* vol 25) (Heidelberg: Springer)
[21] Brühwiler P, Maxwell A, Puglia C, Nilsson A, Andreson S and Martenson N 1995 π^* and σ^* excitons in C-1s absorption of graphite *Phys. Rev. Lett.* **74** 614
[22] Han K-H, Spemann D, Esquinazi P, Höhne R, Riede V and Butz T 2003 Ferromagnetic spots in graphite produced by proton irradiation *Adv. Mater.* **15** 1719–22
[23] Mertins H-C, Oppeneer P M, Valencia S, Gudat W, Senf F and Bressler P R 2004 X-ray natural birefringence in reflection from graphite *Phys. Rev.* B **70** 235106
[24] Carlisle J, Blankenshop S, Termminello L, Jia J, Callcott T, Ederer D, Perera R and Himpsel F 2000 Crystal-momentum-resolved electronic structure of solids using resonant soft-x-ray fluorescence spectroscopy *J. Electron Spectrosc. Relat. Phenom.* **110** 323
[25] Nikitin A, Ogasawara H, Mann D, Denecke R, Zhang Z, Dai H, Cho K and Nilsson A 2005 Hydrogenation of single-walled carbon nanotubes *Phys. Rev. Lett.* **95** 225507
[26] Nikitin A, Nåslund L-A, Zhang Z and Nilsson A 2008 C–H bond formation at the graphite surface studied with core level spectroscopy *Surf. Sci.* **602** 2575
[27] Rosenberg R A, Haija M A and Ryan P J 2008 Chiral-selective chemistry induced by spin-polarized secondary electrons from a magnetic substrate *Phys. Rev. Lett.* **101** 178301
[28] Reichart P *et al* 2006 3D-hydrogen analysis of ferromagnetic microstructures in proton irradiated graphite *Nucl. Instrum. Methods Phys. Res.* B **249** 286